A NOVEL BIOMEMS DEVICE FOR EFFICIENT ON-CHIP SINGLE CELL LOADING AND 3D ROTATION

Liang Huang[1], Peng Zhao[1], Shengtai Bian[2], Guanya Shi[3], Peng Liu[2], Song Zong[1] and Wenhui Wang[1]*

[1] State Key Laboratory of Precision Measurement Technology and Instrument, Department of Precision Instrument, Tsinghua University, Beijing, China

[2] Department of Biomedical Engineering, Tsinghua University, Beijing, China

[3] Department of Automotive Engineering, Tsinghua University, Beijing, China

ABSTRACT

This paper reports a novel bioMEMS device that integrates mechanical constriction for single cell trap in the channels, which are enclosed by thick (or 3D) C-PDMS (carbon-black-PDMS) electrodes and bottom planar transparent electrode for dielectrophoretic (DEP) cell manipulation. Leveraging hydrodynamics and dieletrophoresis, this simple biomedical microsystem enables more efficient loading of one single cell in place and controllable 3D cell rotation than before.

INTRODUCTION

Single cells need to be rotated in many scenarios [1, 2], such as cell characterization, sorting, injection, and enucleation. DEP methods, combined with microfluidic technology, are applied more rapidly than before in biological fields [3, 4]. When used for cell rotation, DEP technology has long been configured in such a way that several (normally four) planar electrodes are formed, like house walls, enclosing a virtual electric-field-filled chamber or cage, inside which the cell rotates. The planar electrodes can only induce 1D cell rotation about the Z-axis. Furthermore, the DEP effect decays sharply in spaces that have a longer distance from the electrode edge, so the effective working area for planar electrodes is limited. However, most DEP methods are based on planar electrodes, which lead to spatially-attenuated DEP effect and thus limited effective working area [5, 6]. Therefore a device [7] was fabricated with a top-open chamber enclosed by 0.5-mm-thick 3D electrodes.

Recently a new device [8] was proposed for solving the remaining problem of loading one single cell at 10 μm scale in place, by adding a hydrodynamics-based single cell trap module [9, 10] above the rotation chamber, which was further scaled-down to accommodate the cell size and enclosed by 100-μm-thick liquid metal electrodes. However, the structure and fabrication of the device cause two problems, i) multiple cells would fall down on the chamber, and ii) high voltage was required to compensate for weak electric strength attenuated by insulating PDMS in the chamber. Correspondingly, we re-designed the structure by placing the trap module on the same layer as the thick electrodes, and fabricated the device using C-PDMS. The new design of the chip platform integrates microfluidic and 3-D cell rotation electrodes together, which has greatly improved the controllability and applicability.

DEVICE DESIGN

The new microfluidic device integrates single cell trap and 3D controllable rotation both on one layer (Fig. 1(a)). Single cell trap is to be achieved by the two V-shaped pillars, while cell rotation by four 3D C-PDMS electrodes and one bottom ITO electrode patterned on glass substrate. Enclosed by the C-PDMS electrodes, the horizontal microchannel has an inlet and an outlet for cell medium loading, while the perpendicular channel is dead-ended only for electrode fabrication. The 3D electrodes are fabricated with C-PDMS (the mixture of carbon black and PDMS) that retains high conductivity and PDMS properties by photolithography. Fig. 1(b) is the photograph of the fabricated device.

To load one single cell, cell medium would be streamed along the flow and only one cell trapped by the opening of the V-shaped pillars, then back-flowed to the right side of the chamber, and finally stabilized inside the chamber where the hydrodynamic force balances the DEP force. To rotate this single cell, different signal configurations are applied on the five electrodes to produce a rotating electric field and thus positive or negative torque.

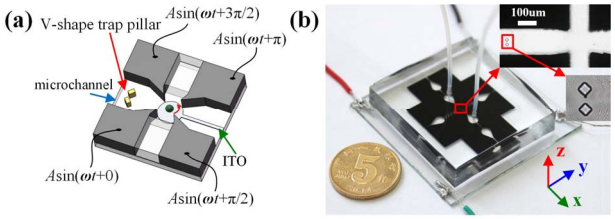

Fig. 1. The proposed bioMEMS device. (a) Concept design. (b) Photograph of the fabricated device with C-PDMS electrodes. The width and height of microchannels are 200 μm×100 μm. The rotation chamber is about 100 μm×100 μm×100 μm. The V-shape configured pillars are 25 μm×25 μm ×25 μm, with an opening of 10 μm for single cell trap.

DEVICE FABRICATION

Fig. 2 illustrates the fabrication procedure for the device. Firstly a mold was fabricated. A 150-μm-thick layer of SU-8 (SU-8-2075, MicroChem Corp.) was first spin-coated and photo patterned to obtain a channel mold. C-PDMS was then plastered on the mold with a blade to remove the excess of conductive polymer. After curing (80◦C, 30 min), pure PDMS was poured on the mold and then cured again. Finally, the PDMS/C-PDMS channel was unmolded and bonded to an ITO glass substrate with special electrical pattern and V-shaped pillars (SU-8 2075). The special electrical pattern of ITO glass was fabricated by photolithography and wet etching, providing electrical contact pads with the C-PDMS electrodes for external wiring. The bottom electrode also was formed by ITO glass. Oxygen plasma was performed to enhance the bonding of ITO glass and C-PDMS.

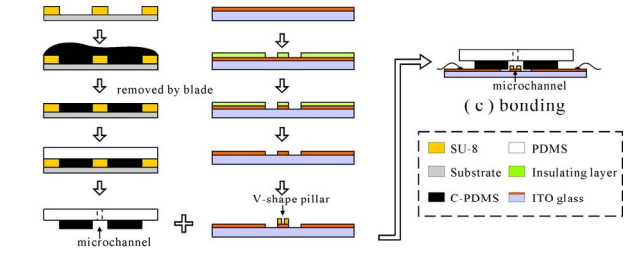

Fig. 2. Schematic diagram of the fabrication process of the bioMEMS device. The microchannels are walled by C-PDMS electrodes. (a) The fabrication process of 3D electrodes and microchannel. (b) The fabrication process of the bottom ITO electrode and the V-shaped trap pillars. (c) Device bonding and wiring.

EXPERIMENT SETUP AND MATERIALS

The experiment setup includes an inverted microscope (Nikon Eclipse Ti-U), a two-channel function generator (AFG3052C; Tektronix) for creating the nDEP signals to load the cell, a four-channel arbitrary waveform generator (TTi12104; Tabor Electronics) for the rotation signals, an oscilloscope (DPO2024B; Tektronix), and a video recording system using a CCD camera with a frame rate of 100Hz (asA640; Basler). The device was placed on the microscope stage, with electric wires connected to two function generators. Cell medium was driven by gravity force, i.e., the syringe as the medium reservoir was adjusted with a relative height compared to the microfluidic device to provide a driving force.

HeLa and C3H10 cells with the diameter of about 8~14μm were used in our experiments. Originally the cells were adherent on the culture substrate. After trypsinized to suspension state, cells were centrifuged at 700×g for 5min to separate the enzyme solution from the cell medium.

The buffer solution should have a low conductivity which can reduce Joule heating exerted by the applied ac signals and also decrease the operating frequency range of the ac signals. The electric conductivity of solution was measured using a conductivity meter (S230-K; Mettler Toledo). In our experiment, DI (deionized) water (conductivity ≈ 6.4μS/cm) was used as the buffer solution to dilute the suspended cells.

EXPERIMENTAL RESULTS

Single cell capture and release

The suspension cell solution was driven by gravity force. Once one cell was trapped by the V-shaped pillars, other cells would not be able to be trapped by the pillars and thus were washed away by flushing cell solution. And then, the captured cell was released by back flow of culture solutions, which was achieved by placing the syringe lower than the microfluidic device. Fig. 3(a), (b) show one single cell was trapped by the V-shape pillars and released by back flow. After the single cell released from the trap pillars and flowed to the intersection, nDEP force (Vp-p=15V, *f*=600kHz) was induced by applying ac signal on the sidewall electrodes and other electrodes were left floating. The nDEP force gets increased as the distance gets closer to the electrodes. When the nDEP force is greater than stoke force; the cell was stopped (Fig. 3 (c)). Under a certain flow rate, the equilibrium location of the cell can be controlled by changing the ac amplitude to adjust the nDEP force. Fig. 3(d) shows the spatial distribution of the gradient of electric field squared and Fig. 3(e) plots the distribution of the DEP force alone the line *A*-*A*. The peak value of the DEP force could shift left as the ac amplitude is increased. In order to ensure the equilibrium position of the cell is in the chamber center, the ac amplitude was adjusted according to the real-time observation in microscope.

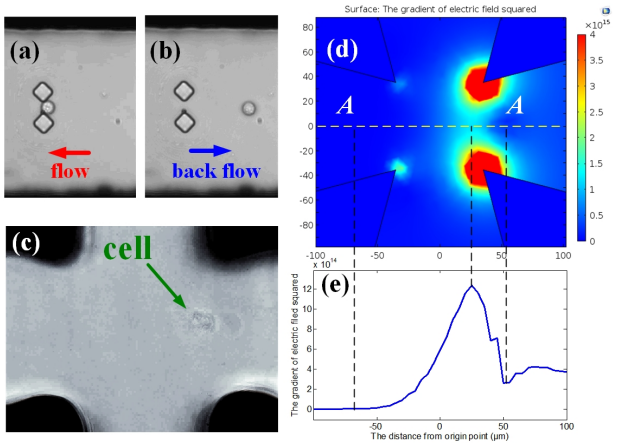

Fig. 3. Single cell loading procedure. (a) One single cell is captured by the V-shaped pillars. (b) The captured cell is released by back flow. (c) The released cell is stopped by DEP force and then back to the rotation chamber at force equilibrium point. (d) Top view of the distribution of gradient of electric field squared. (e) The strength of gradient of electric field squared along the fluidic streamline for DEP force calculation.

Effects of in-plane cell rotation

The cell rotated about Z-axis in the device chamber through applying ac signals to the four sidewall electrodes. In experiment, no rotation was observed in the adjustable frequency range of 100 kHz~10 MHz when the amplitude was below 5V. Clockwise and anticlockwise rotation was achieved for the amplitude of 5V, as shown in Fig. 4(a), (b). As shown in Fig. 4(c), when the frequency was increased in the range from 100 kHz to 10 MHz, a change in the rotation rate was observed. The rotation rate versus frequency curve has a characteristic similar to a band-pass filter. There exists only one peak rotation rate (~1200°/s for amplitude of 14 V and ~600°/s for 8 V) in the measured frequency range.

Under the same frequency, the rotation rate changed as amplitude. Fig. 4(d) shows the curve of rotation rate versus the amplitude. Higher signal amplitude results in a faster rotation. The rotation rate at 14V is nearly six times compared to that at 5V. When the amplitude is greater than 14.5V, electrolysis would happen.

Effects of rolling cell rotation

The rolling cell rotation can be achieved by applying ac signals to the bottom electrode and two sidewall electrodes. The phase shifts between the electrodes were set to 120°. When the amplitude of ac signal is below than

7V, the single cell did not have rolling rotation. Otherwise, the cell started rolling rotation as shown in Fig. 5(a). The relationship between the rotation rate and frequency is similar to in-plane rotation and plotted in Fig. 5(b). There is a peak value at 700 kHz and the rotation spectrum resembles a Gaussian distribution. But the frequency range becomes narrower compared to that of the in-plane rotation. The reason may be the asymmetry of electrodes distribution and the influence of gravity force.

Similarly to in-plane rotation, higher signal amplitude causes faster rolling rotation. The effect of varying amplitudes on the rolling rotation rate was investigated and the results are shown in Fig. 5(c). The directions of rolling rotations about X-axis or Y-axis could be obtained by interchanging the signals configuration of electrodes.

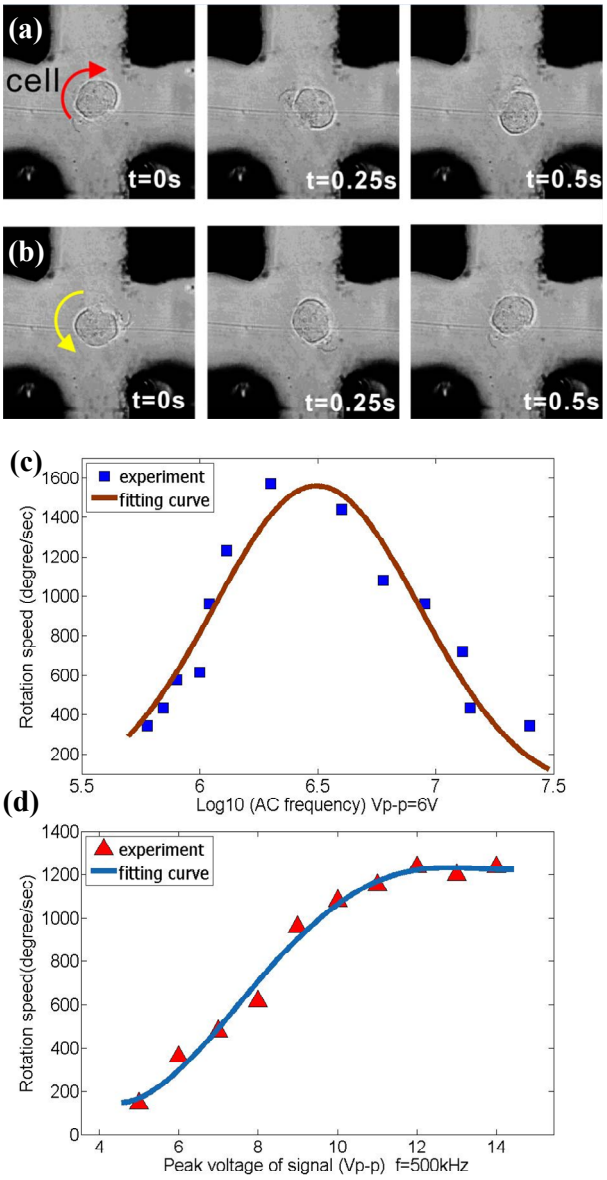

Fig. 4. In-plane cell rotation. (a) Temporal snapshots of the in-plane cell (Vp-p=10V, f=600kHz). (b) Cell rotation speed in relation to applied frequency. (c) Cell rotation speed in relation to signal amplitude (f=500kHz).

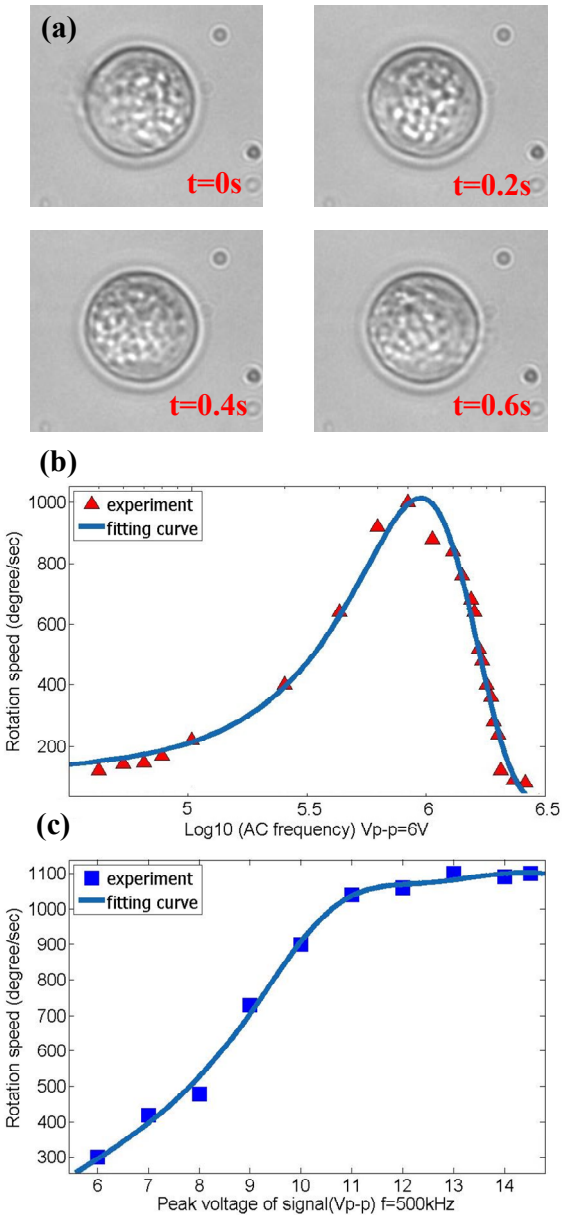

Fig. 5. Rolling cell rotation. (a) Temporal snapshots of the rolling cell (Vp-p=10V, f=600kHz). (b) Cell rotation speed in relation to applied frequency. (c) Cell rotation speed in relation to signal amplitude (f=500kHz).

Rotation manipulation outside of the chamber

When the cell was out of the chamber, we also observed interesting rotation patterns happen as expected by simulated electric field distributions. Fig. 6(a) shows the signal scheme in which the signals with phase shift of 120° are respectively applied to electrodes for rolling rotation. In-plane rotation and rolling rotation could occur respectively in the two neighboring regions separated by the boundary between the bottom electrode and non-electrode areas, outlined by the dashed line in Fig. 6(b). The electric fields exhibit different rotating patterns in the non-electrode and electrode regions. In particular, the electric field in the non-electrode region rotates about Z-axis and the electric field in the electrode region rotates about X-axis. So cells in the two regions have in-plane rotation and rolling rotation, respectively, as shown in Fig. 6(b).

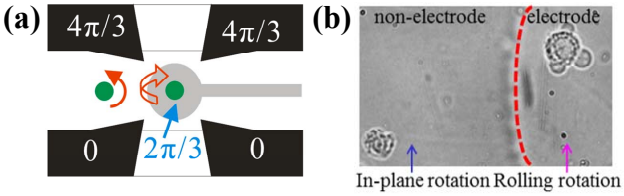

Fig. 6. Rotation pattern in the region left to the chamber. (a) The signal configuration is analyzed to produce in-plane and rolling rotation patterns separated by the boundary of bottom electrode. (b) Experimental results. Two cells did in-plane rotation and rolling rotation separately around the boundary.

When the cell was located in the region right to the chamber (Fig. 7(a)), the cell moved towards the sidewall electrode for equilibrium. It can adaptively stay at the position where the force is balanced in both horizontal and vertical directions. The position of the cell can be controlled by adjusting the amplitude of voltage, but always between the side-wall electrode and the bottom one. In this region, the electrical field rotates in the rolling pattern, and thus the single cell does rolling rotation as well (Fig. 7(b)). In experiment, we observed the rotation rate reach about ~240°/s.

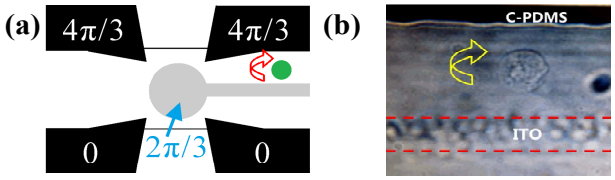

Fig. 7. Rotation pattern in the region right to the chamber. (a) The signal configuration is analyzed to produce rolling rotation in the region enclosed by one 3D electrode and the bottom electrode. (b) Experimental results.

CONCLUSION

This paper presents a new device for single cell loading and 3D rotation. C-PDMS was used to fabricate rather thick side-wall electrodes with simple processing steps and low cost. The device works to trap a single cell with high efficiency by utilizing V-shaped pillars in microchannel, based on the least flow resistance path principle. And the DEP force induced by side-wall electrodes can translocate the cell released from the trap in the chamber center. To solve the issues of water electrolysis, bubble formation and joule heating, the signals are optimized to have frequency from 100kHz to 10MHz and amplitude from 5V to 14.5V. Interestingly, the cell can rotate in and out of the rotation chamber with patterns. By applying different ac signals, stable and controllable 3D cell rotation can be achieved with optimized frequency and amplitude.

In summary, this new device has lots of advantages such as better controllability, simpler processing and lower cost. The 3D cell rotation bioMEMS platform could be an enabling manipulation tool for many interesting biological studies.

ACKNOWLEDGEMENTS

This work was supported by the NSFC (no. 61376120), the National Key R&D Program (no. 2016YFC0900200), the National Instrumentation Project (no. 2013YQ19046701), and the One-Thousand Young Talent Program of China.

REFERENCES

[1] C. Leung, Z. Lu, X.P. Zhang and Y. Sun, "Three-dimensional rotation of mouse embryos," *IEEE Transactions on Biomedical Engineering*, vol. 59, no. 4, pp. 1049-1056, 2012.

[2] D. Ahmed, A. Ozcelik, N. Bojanala, N. Nama, A. Upadhyay, Y. Chen, W. Hanna-Rose, and T. J. Huang, "Rotational manipulation of single cells and organisms using acoustic waves," *Nature Communications,* vol. 7, p. 11085, 2016.

[3] S. Han, Y. Joo and K. Han, "An electrorotation technique for measuring the dielectric properties of cells with simultaneous use of negative quadrupolar dielectrophoresis and electrorotation," *The Analyst,* vol. 138, p. 1529, 2013.

[4] Y. Kung, K. Huang, W. Chong, and P. Chiou, "Tunnel dielectrophoresis for tunable, single-stream cell focusing in physiological buffers in high-speed microfluidic flows," *Small,* vol. 12, pp. 4343-4348, 2016.

[5] S. Lin, Y. Tung and C. Lin, "A frequency-control particle separation device based on resultant effects of electroosmosis and dielectrophoresis," *Applied Physics Letters,* vol. 109, p. 053701, 2016.

[6] N. Chen, C. Chen, M. Chen, L. Jang, and M. Wang, "Single-cell trapping and impedance measurement utilizing dielectrophoresis in a parallel-plate microfluidic device," *Sensors and Actuators B: Chemical,* vol. 190, pp. 570-577, 2014.

[7] P. Benhal, J. G. Chase, P. Gaynor, B. Oback, and W. Wang, "AC electric field induced dipole-based on-chip 3D cell rotation," *Lab on a Chip,* vol. 14, p. 2717, 2014.

[8] L. Huang, L. Tu, X. Zeng, L. Mi, X. Li, and W. Wang, "Study of a microfluidic chip integrating single cell trap and 3D stable rotation manipulation," *Micromachines,* vol. 7, p. 141, 2016.

[9] D. Jin, B. Deng, J. X. Li, W. Cai, L. Tu, J. Chen, Q. Wu, and W. H. Wang, "A microfluidic device enabling high-efficiency single cell trapping," *Biomicrofluidics,* vol. 9, p. 014101, 2015.

[10] L. Mi, L. Huang, J. Li, G. Xu, Q. Wu, and W. Wang, "A fluidic circuit based, high-efficiency and large-scale single cell trap," *Lab on a Chip,* DOI: 10.1039/C6LC01120A, 2016.

CONTACT

*W.H. Wang, tel: +86-10-62797275;
wwh@tsinghua.edu.cn